Photoswitching of Green mEos2 by Intense 561-nm Light Perturbs Efficient Green-to-Red Photoconversion in Localization Microscopy

Daniel Thédié, Romain Berardozzi, Virgile Adam, Dominique Bourgeois[*].

SUPPLEMENTARY METHODS

mEos2 immobilization for *in vitro* experiments

Purified mEos2 was diluted to either micromolar (ensemble experiments) or nanomolar (single-molecule experiments) concentration in a solution of 1% polyvinyl alcohol (PVA, Sigma Aldrich, USA) in PBS buffer pH=7.4. The mEos2-containing PVA was then spread to form a uniform thin layer on a coverslip thoroughly cleaned with a UV Ozone Cleaning System (HELIOS-500, UVOTECH Systems), and let to harden at room temperature for 5 minutes. Control experiments in protein-free PVA film showed few red contaminant molecules (~3% of total molecules imaged in a mEos2-containing PVA film, Figure S12). The same procedure was used to study mEos4b, mEos3.2 and Dendra2.

Transformation and fixation of bacteria

BL21 *E. coli* strains were transformed with a mEos2/pRSET-A plasmid (Life Technologies, USA) and colonies were cultured in LB medium supplemented with 1 mg/mL ampicillin for 4 hours at 37°C under agitation. For single-molecule experiments, pelleted bacteria were washed twice with 1X phosphate buffered saline buffer pH=7.4 (Dulbecco's PBS, Gibco, USA) before fixation with a 4% formaldehyde (Sigma Aldrich) solution for 1 hour at room temperature. After fixation, bacteria were washed twice and diluted to reach a final cell density on the coverslip of around 10-20 bacteria per ~30 x 30 µm² field of view. Bacterial suspensions were deposited and incubated on chitosan-coated coverslips (chitosan from crab shell 48-165, Sigma Aldrich) for 1 hour at room temperature. The surface was washed with PBS and the cells deposited in the same buffer prior to sealing the coverslide with valap (vaseline-lanolin-paraffin wax mix) to avoid drying. For ensemble-level experiments, 5 µL of bacterial culture were directly spread on an agarose-coated coverslip. Control coverslips prepared according to these protocols but without bacteria showed very few blinking molecules.

Microscope setup and data acquisition

Ensemble and PALM data were acquired on a home-built setup based on an Olympus IX81 inverted microscope equipped with a x100 1.49 NA oil-immersion apochromatic objective lens (Olympus, Japan). Widefield illumination was achieved by focusing the diode-pumped solid state 405-nm (CrystaLaser, USA), 488-nm (Spectra Physics, USA) and 561-nm (Cobolt Jena, Sweden) laser beams to the back focal plane of the objective. Intensities of laser illuminations at the sample were tuned by an acousto-optical tunable filter (AOTF, AA Opto Electronic, France). Fluorescence images were acquired with an Evolve 512 back-illuminated EMCCD camera (Photometrics, USA) controlled by the Metamorph software (Molecular Devices, USA). Beam profiles were recorded before each experiment using a coverslip uniformly marked with a

fluorescent dye. Near circular polarization of the laser beams was ensured by inserting a polychromatic quarter-wave plate downstream the AOTF.

Ensemble experiments
Experiments at the ensemble level were performed by alternating 50 ms of fluorescence readout by weak 488-nm light and 900 ms of exposure to either 488-, 561-, or 405-nm light (Figure S1).

Single-color PALM experiments
All PALM data were collected with continuous 405-nm and 561-nm light illumination or continuous 561-nm light illumination only, using a frametime of 30 ms.

2-color PALM experiments
To acquire 2-color PALM data, green and red fluorescence emissions were split prior to detection using a dichroic filter (Semrock, USA), and directed each to a different half of the EMCCD detector. Images were acquired using alternate 488- and 561-nm illumination, with a 25 ms exposure time.

Simulations

In-house made Matlab-based PALM simulation software

Palm simulations were performed as described in Avilov et al.[1] In brief, the photophysics of single-molecules was simulated according to Scheme 1. The simulation also included a large panel of experimental parameters, such as fluorophore density, dipole orientation (as described in ref 2), laser power density and polarization, poissonian background noise, objective properties, and EMCCD parameters.

Data processing

Determination of switching rates and off-switching yields from ensemble experiments

Fluorescence levels were measured over a small region of the recorded field of view, so as to ensure homogenous laser intensities. The resulting switching curves were fitted with the model of Scheme S1b using a custom software written in Matlab (Matlab 2015b, The MathWorks, USA), so as to extract rate constants. On-off switching was systematically followed by 1 min of off-on recovery under 405-nm light, in order to evaluate the amount of fluorophores irreversibly bleached or photoconverted. This information was used to set the k_2 rate constant (corresponding to bleaching and photoconversion) to a value consistent with the observed level of fluorescence recovery. Fluorescence off-switching rates under 488-nm readout light only (see Figure S3) were incorporated as fixed rates in the model used for fitting of the off-switching curves under 561-nm light, so as to account for the residual effect of readout light on the fluorescence decays. Furthermore, for each fit it was checked that the Jacobian at the solution was not ill-conditioned, ensuring that all parameters were uncorrelated.
Off-switching quantum yields under 488-nm light were derived from the off-switching rates using excitation rates calculated from extinction coefficients measured in solution and local laser power densities measured from recorded beam profiles.
All experiments were performed in triplicates.

Single-molecule data processing and determination of the phototransformation rates

Single-molecule data were processed as described in Avilov et al.[1] Briefly, after molecule localization using the Thunderstorm plugin for ImageJ[3] and optimal splitting of the fluorescence traces to correct for blinking in the red state of mEos2, cumulative curves of the

newly photoconverted molecules along the dataset were obtained. The kinetic model described in Scheme S1b was fitted against experimental data to extract the phototransformation rates. In PVA triplicate experiments were recorded on distinct regions of a sample, and in bacteria they were obtained from the analysis of different cells present in the field of view.

Tracking photoconversion events at the single-molecule level using a 2-color setup

The acquired 2-color PALM dual-frame datasets were split in green and red datasets. The red single-molecules were localized using the Thunderstorm plugin for ImageJ[3], and their positions corrected for image distortion between the green and red channels using a reference dataset containing fluorescent beads (Tetraspeck T7279, Thermofisher). Reconstitution of the fluorescence traces of the red molecules was achieved as described above. For each of these fluorescence traces, green single-molecules were searched for in the frames preceding the appearance of the red molecule by measuring the average pixel value over a small region (of the order of a PSF area) and comparing this value to the background noise obtained on a bigger neighbouring region. A pixel intensity of 4 times the background noise standard deviation was considered significant for the detection of single-molecules. Assuming a detection efficiency of 100% for the single-molecules in the green channel, and the absence of delayed photoconversion via D_{long}, one expects every newly appearing red molecule to be preceded by a green molecule at a one-frame distance.

(1) Avilov, S.; Berardozzi, R.; Gunewardene, M. S.; Adam, V.; Hess, S. T.; Bourgeois, D. In Cellulo Evaluation of Phototransformation Quantum Yields in Fluorescent Proteins Used as Markers for Single-Molecule Localization Microscopy. *PloS One* **2014**, *9,* e98362.

(2) Duan, C.; Byrdin, M.; Khatib, M. E.; Henry, X.; Adam, V.; Bourgeois, D. Rational Design of Enhanced Photoresistance in a Photoswitchable Fluorescent Protein. *Methods Appl. Fluoresc.* **2015**, *3*, 014004.

(3) Ovesný, M.; Křížek, P.; Borkovec, J.; Švindrych, Z.; Hagen, G. M. ThunderSTORM: A Comprehensive ImageJ Plug-in for PALM and STORM Data Analysis and Super-Resolution Imaging. *Bioinformatics* **2014**, *30*, 2389–2390.

SUPPLEMENTARY SCHEMES AND FIGURES

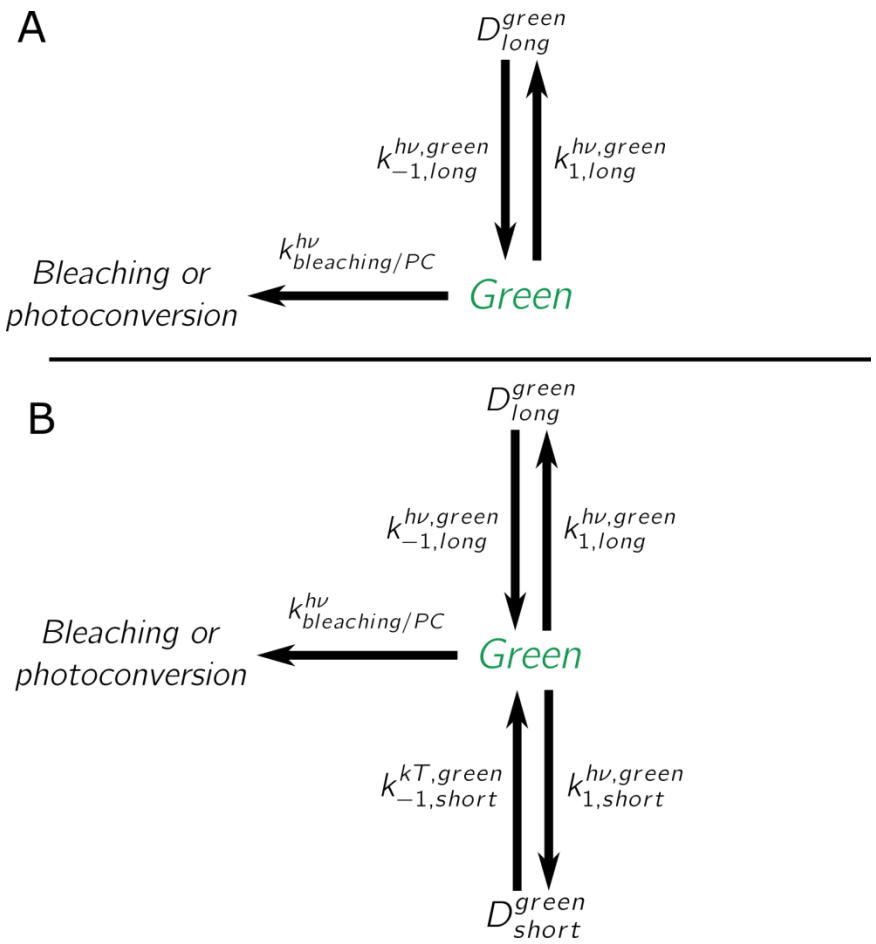

Scheme S1. Kinetic models used for fitting of green mEos2 switching curves**.**

(A) This fitting model includes only one reversible dark-state for the green form of mEos2 (D_{long}), and does not account for the observed on-off switching curves (Figure S7A, C).

(B) This fitting model, corresponding to the model of Scheme 1, includes two reversible dark states, and is able to both fit the experimental data and account for the high level of fluorescence recovery under 405-nm light (FigureS7B, D). The off-on fluorescence recoveries in Figure 1 were fitted using solely the $k_{-1,\,long}$ constant.

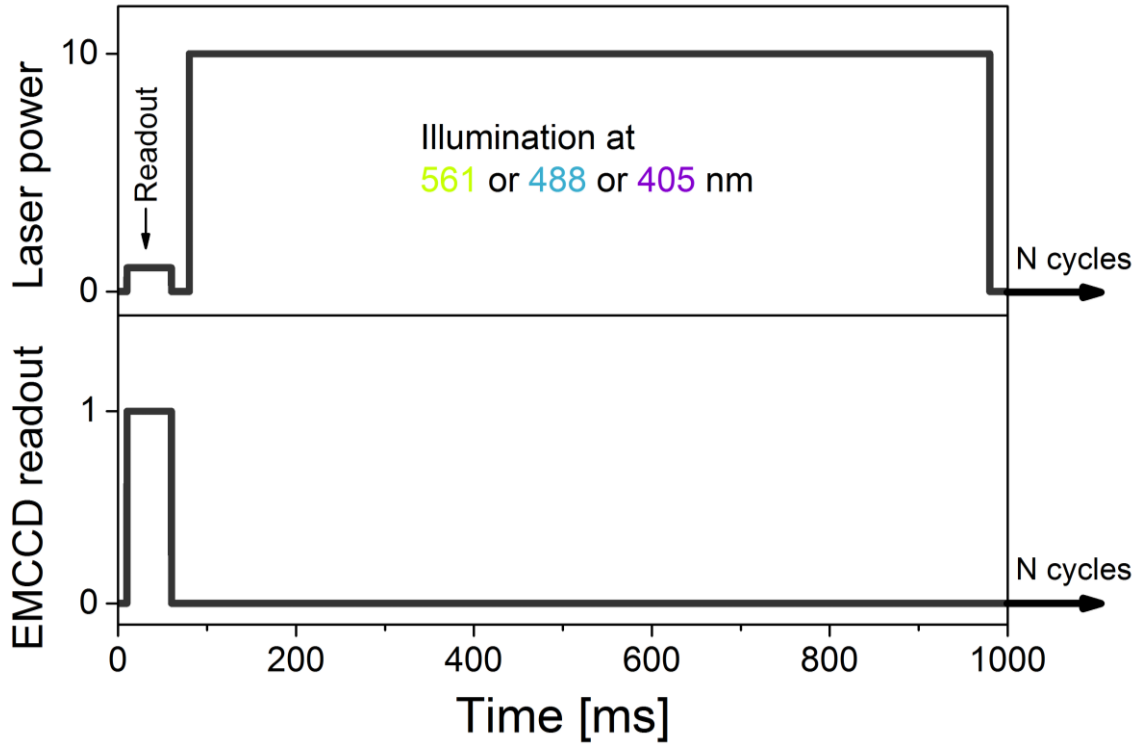

Figure S1. Laser illumination and EMCCD acquisition scheme for ensemble fluorescence experiments.

During ensemble experiments (as reported in Figure 1), fluorescence readout was achieved by weak illumination at 488 nm during 50 ms, followed by actinic illumination at either 561, 488, or 405 nm.

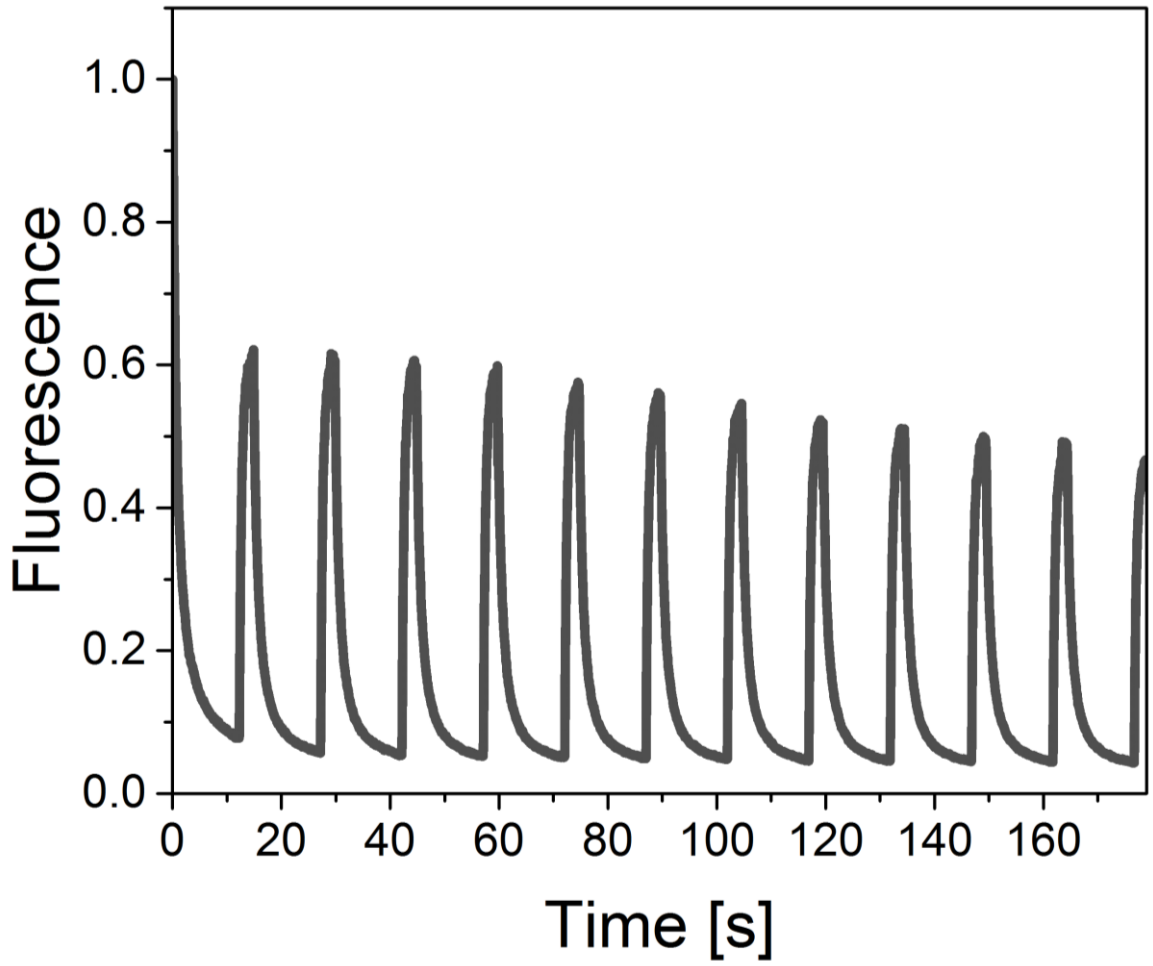

Figure S2. Green mEos2 exhibits the behavior of a reversibly switchable fluorescent protein.

mEos2 embedded in PVA was illuminated with continuous 488-nm and alternating 405-nm light, inducing reversible dark-state formation and recovery to the green form, respectively. Switching could be repeated over several cycles with only moderate photobleaching.

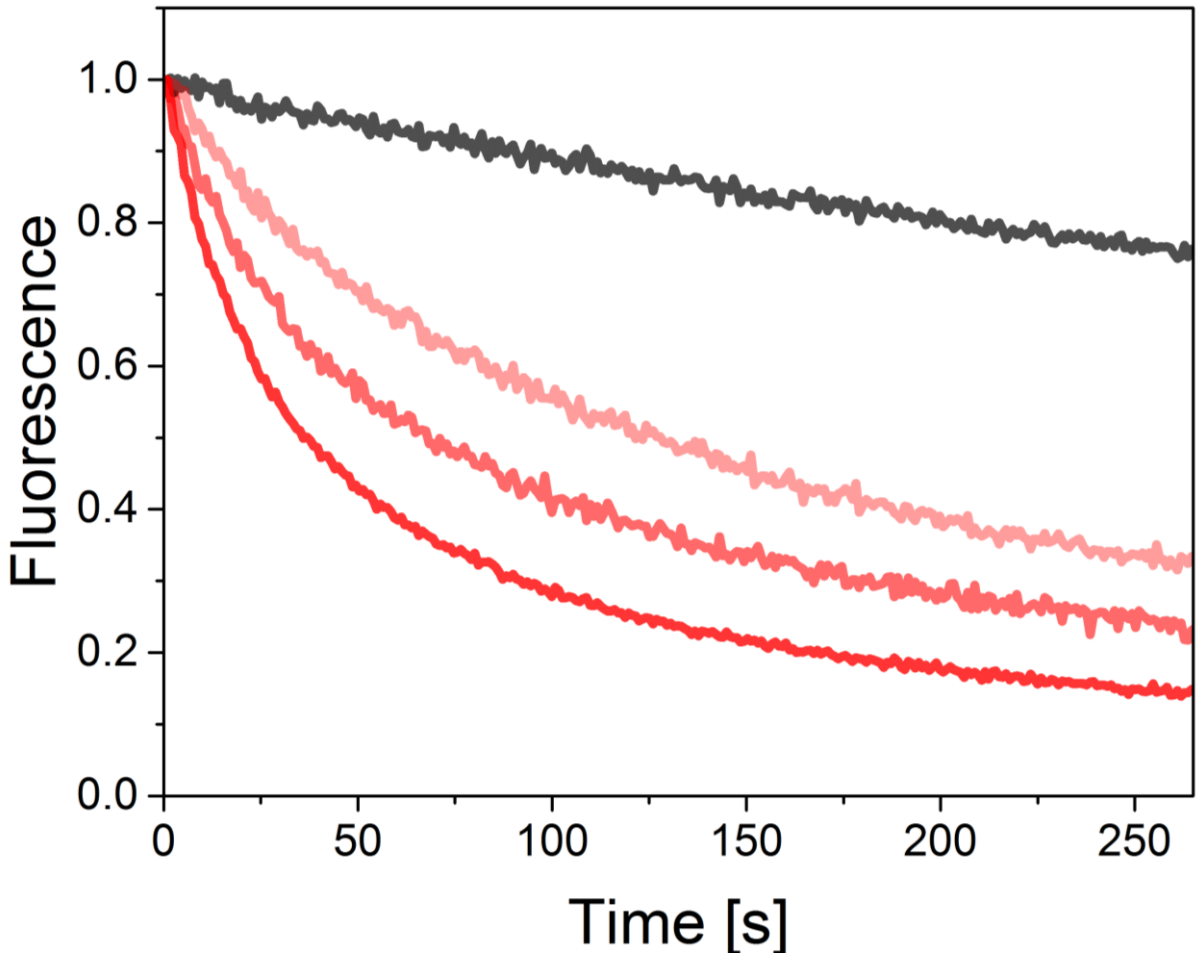

Figure S3. Effect of increasing the power density of 561-nm light on green mEos2 on-off switching kinetics. mEos2 embedded in PVA shows residual switching in the absence of actinic light (black curve), due to the weak fluorescence readout light at 488 nm (0.2 W/cm^2), and leading to the loss of ~20% of fluorescence over 250 s. In presence of increasing intensities of 561-nm actinic light (darker shades of red represent higher 561-nm power density: 1200, 2400 and 3600 W/cm^2), much more pronounced switching occurs.

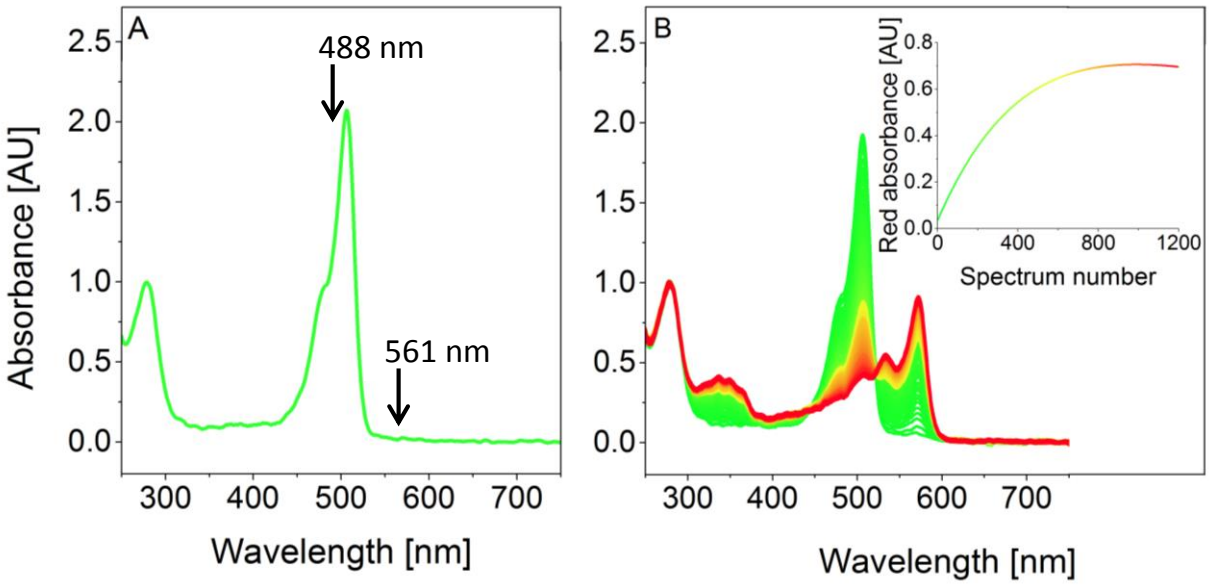

Figure S4. Absorbance spectrum of mEos2 green form.

(A) Absorbance spectrum of green mEos2. Positions of 488- and 561-nm illumination are shown.

(B) Evolution of mEos2 absorbance spectra upon green-to-red photoconversion under 405-nm illumination (green to yellow to red). The absorbance maximum is shifted from 500 to 570 nm, and a clear isosbestic point is visible at 520 nm at the early stages of the experiment. The evolution of the red absorbance (at 572 nm, inset) along the experiment is monophasic (except the onset of photobleaching at late stage of the experiment), indicating the absence of dark-state formation under illumination exclusively at 405 nm.

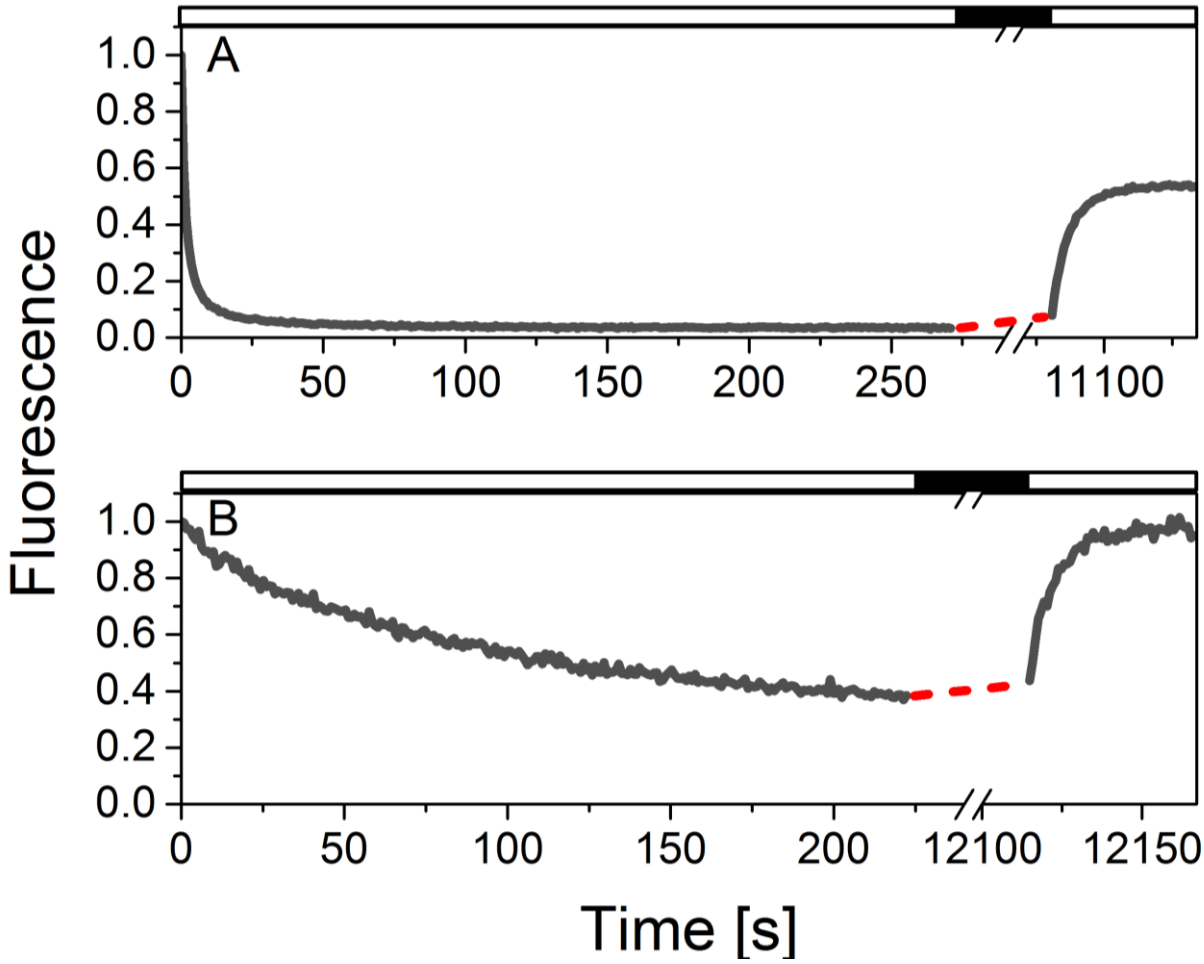

Figure S5. Thermal stability of the dark-states formed under 488-nm and 561-nm illumination.

Green mEos2 embedded in PVA was illuminated at 488-nm (10 W/cm^2, A) or 561-nm (1200 W/cm^2, B) for 250 seconds, and subsequently left in the dark for 3 hours (red dotted lines). At the end of this period, only weak fluorescence recovery could be observed, whereas subsequent faint illumination at 405 nm for 1 minute induced significant fluorescence recovery.

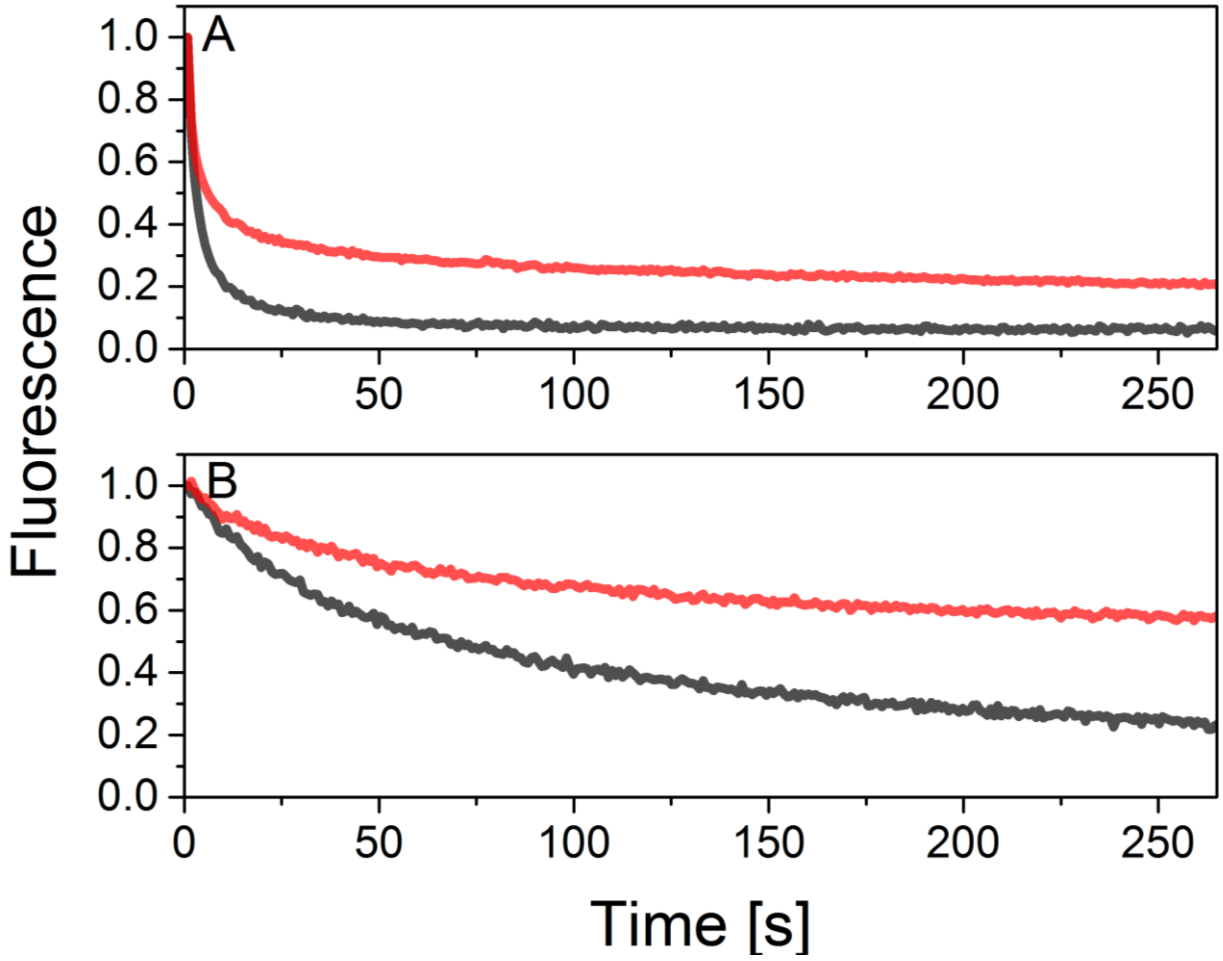

Figure S6. Influence of the pH on mEos2 green fluorescence decay under 488- or 561-nm illumination at the ensemble level.

mEos2 at pH 7 or pH 5 embedded in a 12% polyacrylamide gel was exposed to 488-nm (10 W/cm^2, A) or 561-nm (2400 W/cm^2, B) light. Fluorescence at 525 nm is shown (black curve: pH 7, red curve: pH 5). Lowering the pH significantly slows down the fluorescence decay under both illumination conditions, indicating that 488-nm and 561-nm light both affect the anionic state of mEos2.

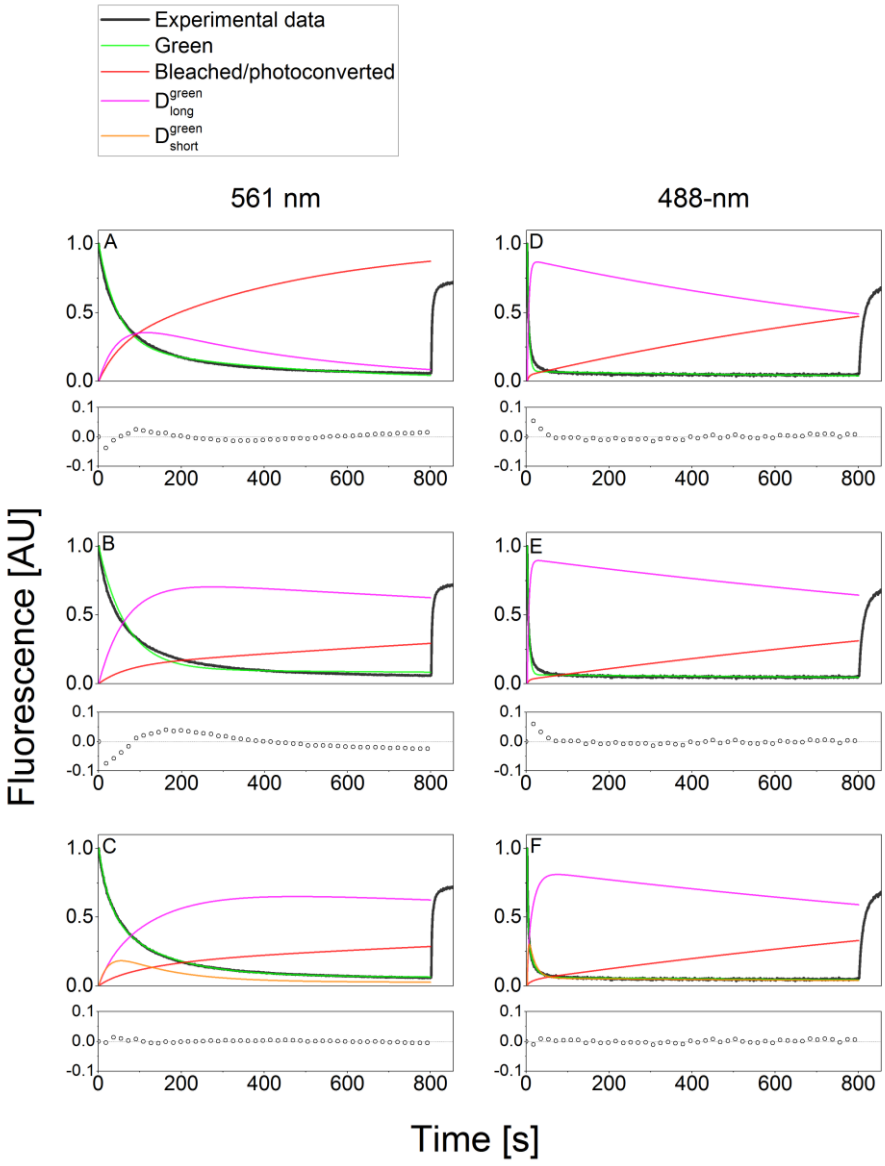

Figure S7. Fitting of green mEos2 on-off switching curves under 561- or 488-nm light with only one dark state (Scheme S1A) fails to account for the experimental data.

(A, D) Fitting with the model of Scheme S1A (green curve) fails to accurately describe the experimental on-off switching curve (black). Moreover, a high level of bleaching and/or photoconversion is predicted (over 80 or 50% under 561- or 488-nm light, respectively, red curves), which is inconsistent with the ~70% fluorescence recovery observed upon subsequent 405-nm illumination. The magenta curve shows the evolution of the reversible dark state population. The lower panels show fitting residuals.

(B, E) Restraining the rate of bleaching/photoconversion to match the amount of fluorescence that cannot be recovered under 405-nm illumination (~30%), the model fails to accurately describe the experimental on-off switching curve.

(C, F) Fitting with the model of Scheme S1b including two reversible dark states (magenta, long-lived and orange, short-lived) matches both the experimental on-off switching curve and the high level of fluorescence recovery upon 405-nm illumination.

Fitting residuals are shown in the bottom panels.

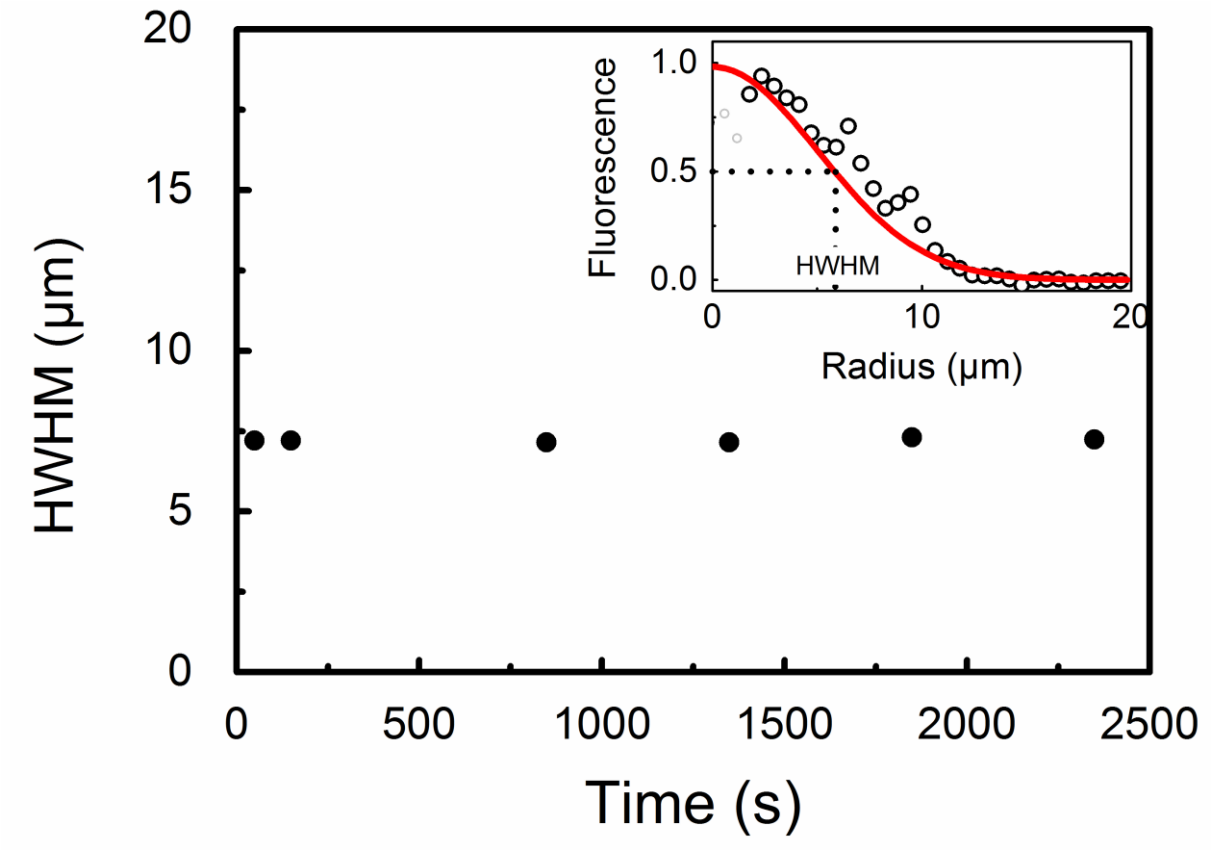

Figure S8. Diffusion kinetics of mEos2 in a PVA thin layer.

A circular region of 20 µm radius of mEos2 embedded in PVA was photoconverted by a 20 ms pulse of 405-nm laser light and red fluorescence was imaged along time using a spinning-disk microscope equipped with a FRAP module. The maximum fluorescence within the photoconverted region was normalized to 1. The distance from the center at which fluorescence is equal to 0.5 (corresponding to the half-width at half maximum (HWHM) of the Gaussian-shaped profile of red fluorescence shown in the inset) is reported (black circles) along time. Thus, within a time scale of 2,500 seconds, red mEos2 molecules do not significantly diffuse within the PVA film.

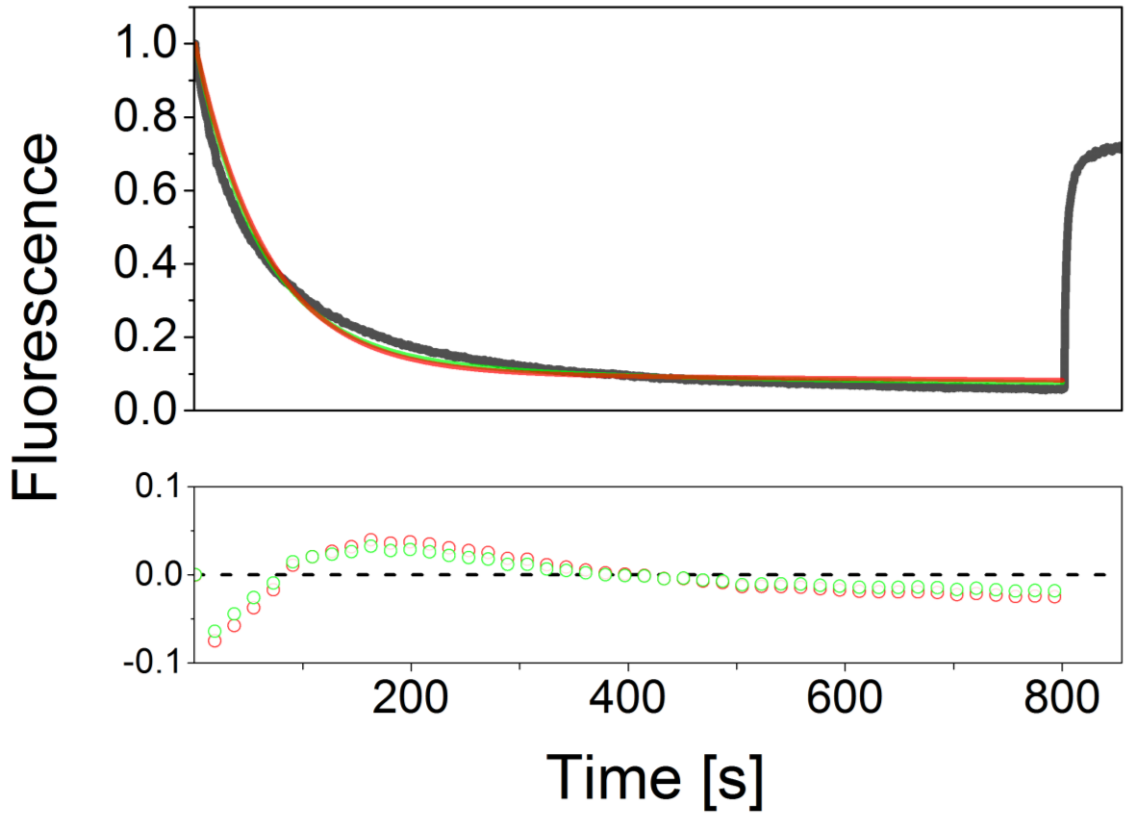

Figure S9. Effect of dipole orientation on mEos2 fluorescence decay.

Fitting of green mEos2 on-off switching under 561-nm illumination (2400 W/cm^2) with the model of scheme S1a, either considering fluorophore rapid tumbling (red curve) or fixed fluorophores (red curve). The bottom panel shows the fitting residuals. The difference in the fit is minor, so that the possibly anisotropic distribution of the fluorophores in PVA does not account for the observed shape of the switching decay.

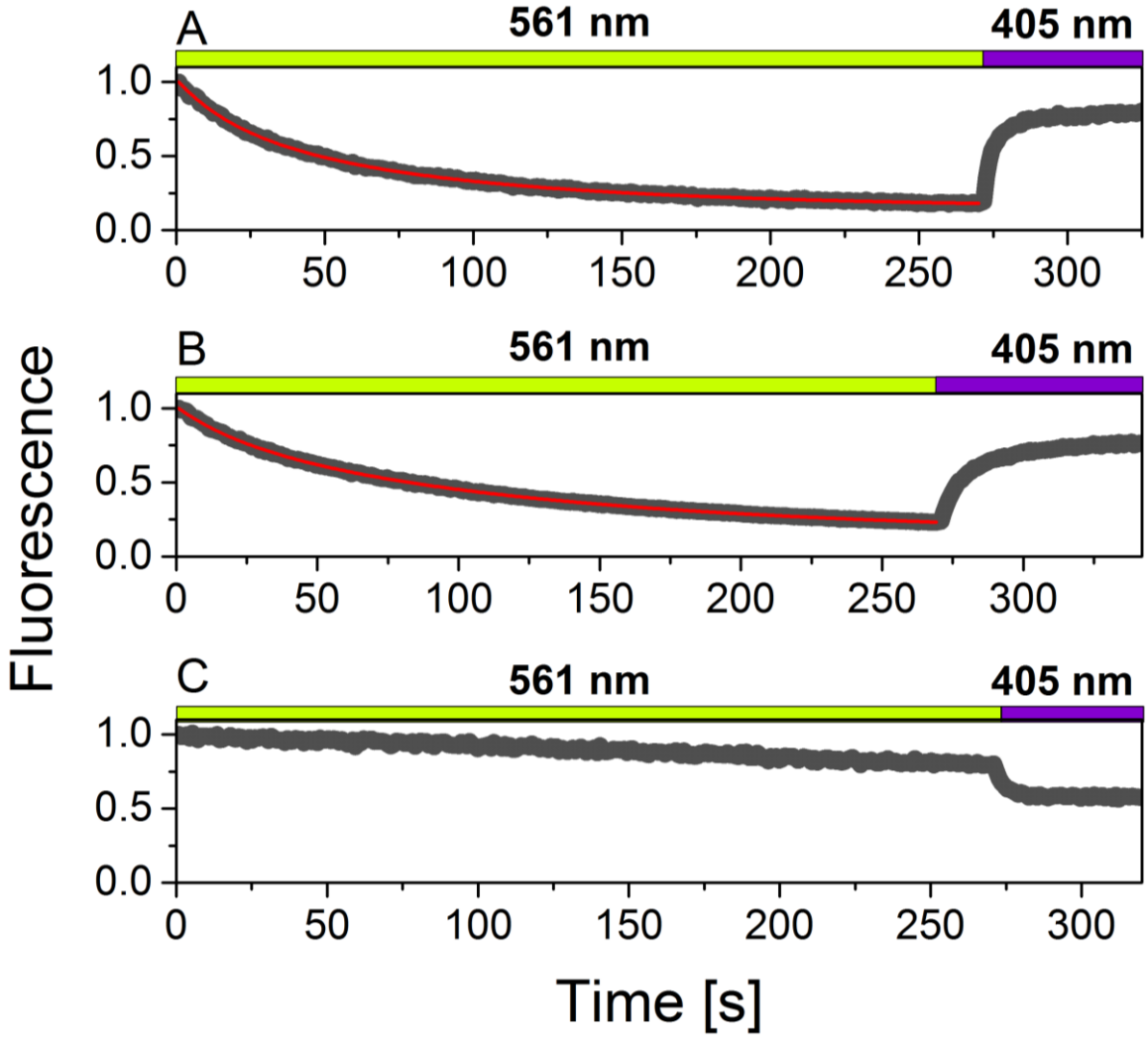

Figure S10. mEos3.2 and mEos4b display similar switching behavior as mEos2, whereas Dendra2 switches less efficiently.

mEos3.2 (A), mEos4b (B) and Dendra2 (C) embedded in PVA were sequentially illuminated by strong 561-nm (2400 W/cm^2) and weak 405-nm light (0.03 W/cm^2). mEos3.2 and mEos4b show a similar behavior as mEos2 (Figure 1B), strongly suggesting that the switching mechanism of mEos2 is a common feature to all EosFP-derived photoconvertible proteins. Both fluorescent decays could well be fitted with the model of Scheme S1B (red curves). Dendra2 switches much more slowly under 561-nm illumination and undergoes further light-induced switching and/or photoconversion or bleaching under weak 405-nm illumination.

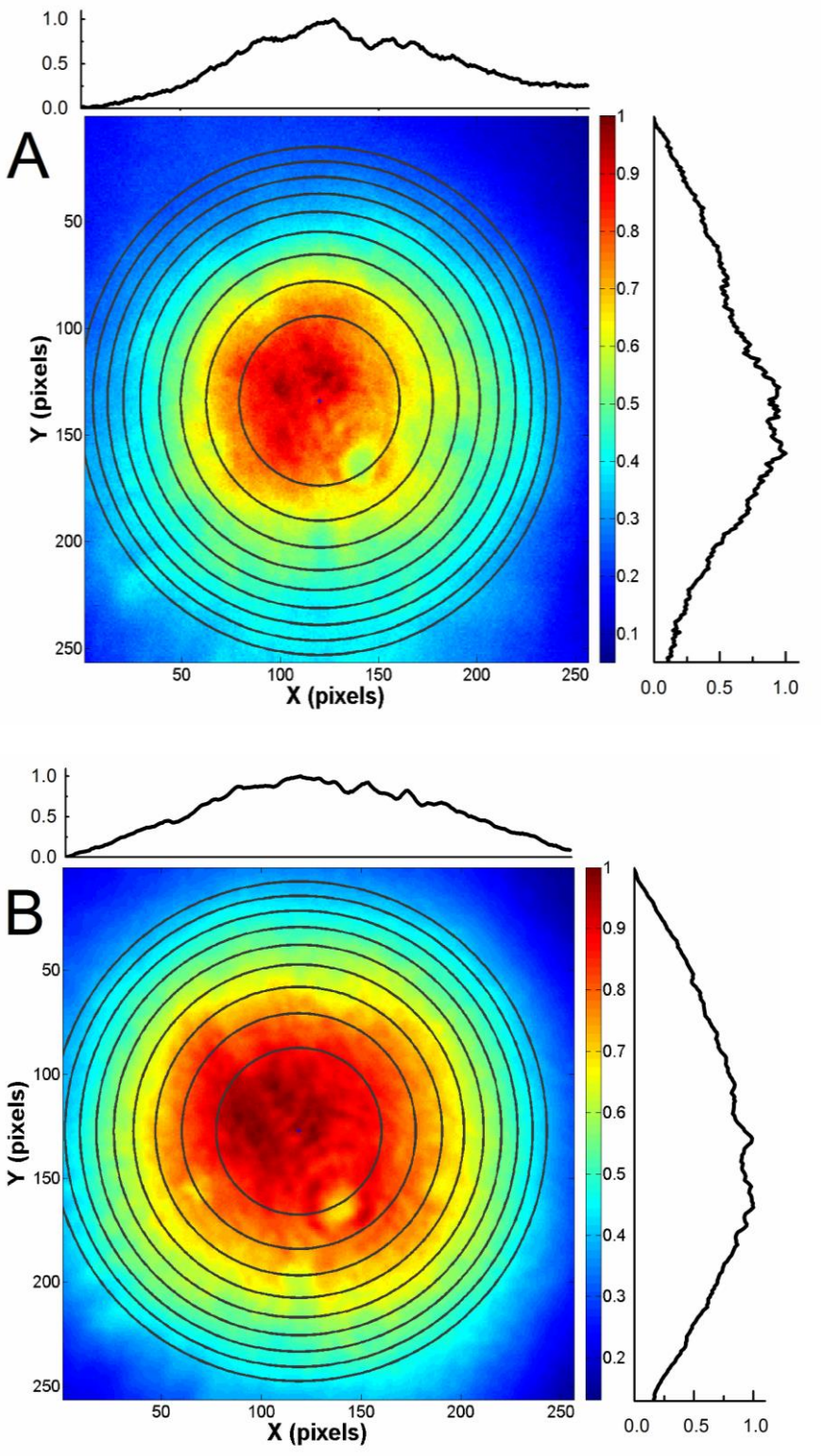

Figure S11. Beam profiles of 405-nm and 561-nm lasers.

For single-molecule data processing in Figure S13, molecules were divided in 10 groups corresponding to the ten regions of the 405-nm (A) and 561-nm (B) laser profiles highlighted by black circles. Each region is considered homogeneous.

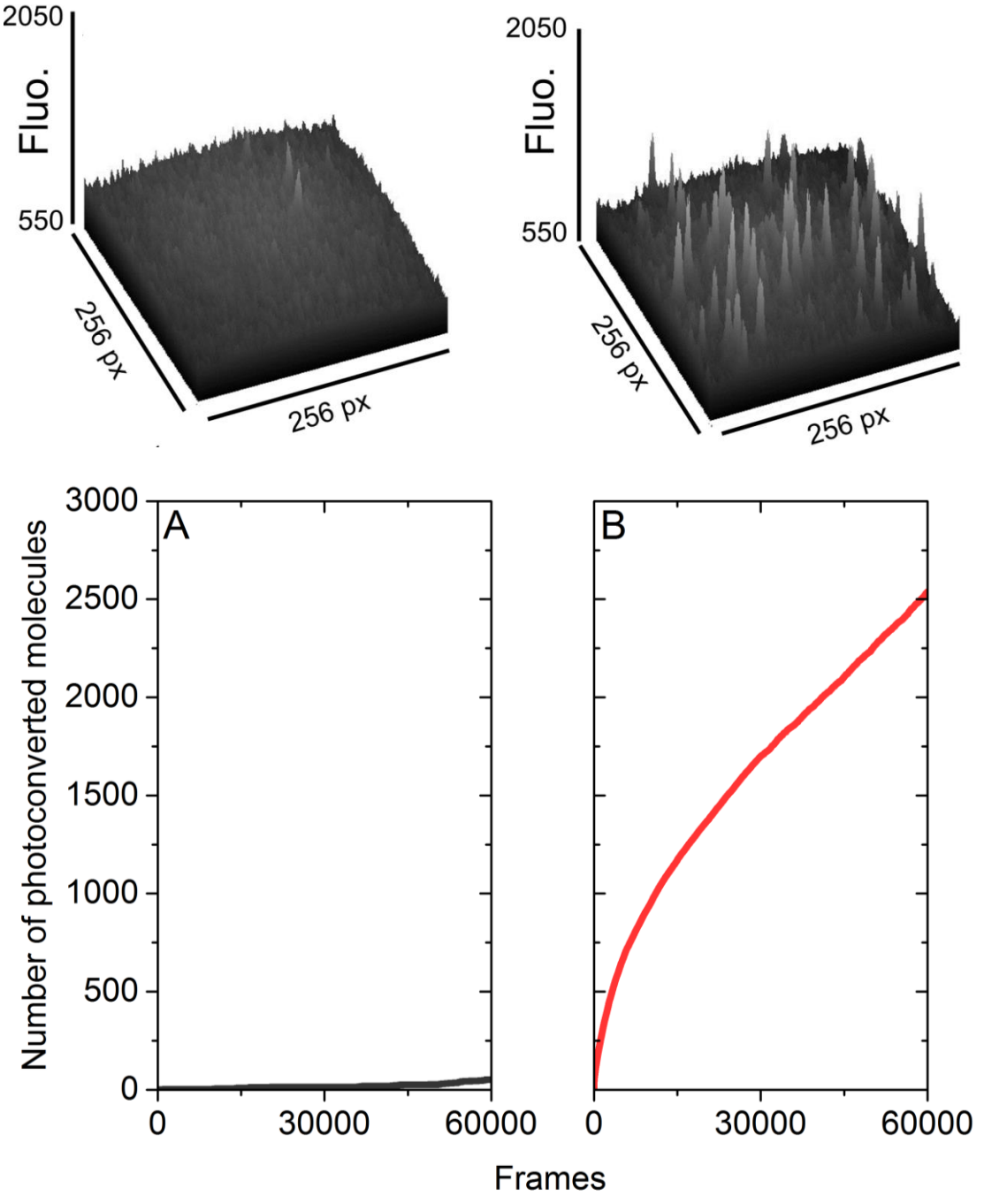

Figure S12. PVA samples contain a negligible amount of red-fluorescent impurities.

(Top): Representative surface plots of fluorescent molecules in a PVA film containing (B) or not (A) mEos2 molecules diluted to nanomolar concentration and obtained under the same illumination conditions (561-nm light). The corresponding cumulative curves of red photoconverted molecules are also shown (bottom). These data suggest that residual impurities are unlikely to alter the cumulative photoconversion curves of Figure 3.

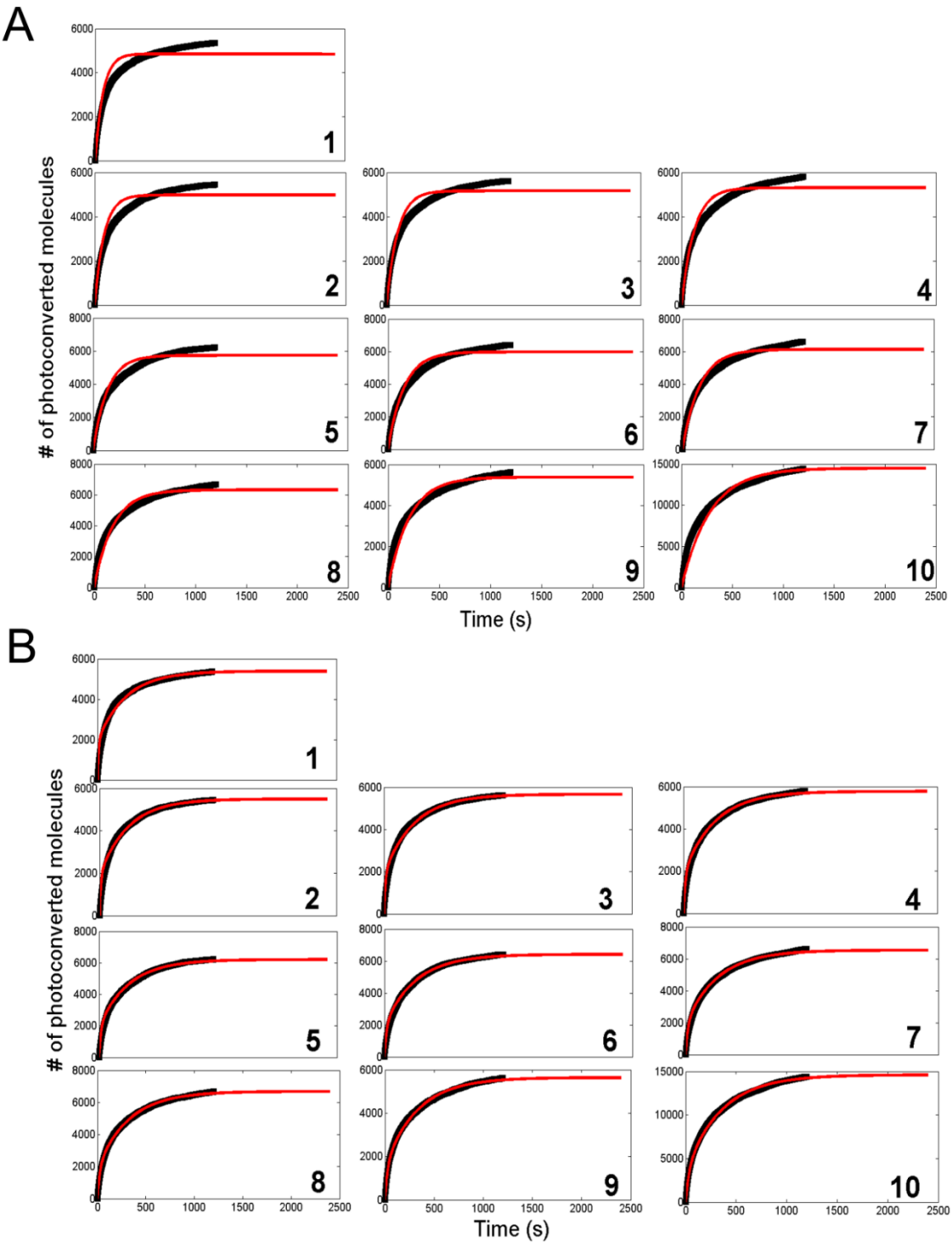

Figure S13. Cumulative photoconversion curves under homogenous laser exposure cannot be fitted by a monophasic model.

Cumulative photoconversion curves (black) are shown for each annular region (1 to 10; see Figure S11). A global kinetic model taking into account the mean laser power density in each region but not accounting for dark-state formation in green mEos2 (monophasic model, red curves) fails to properly fit the data (A), whereas a global model accounting for dark-state formation properly describes the data (red curves) (B).

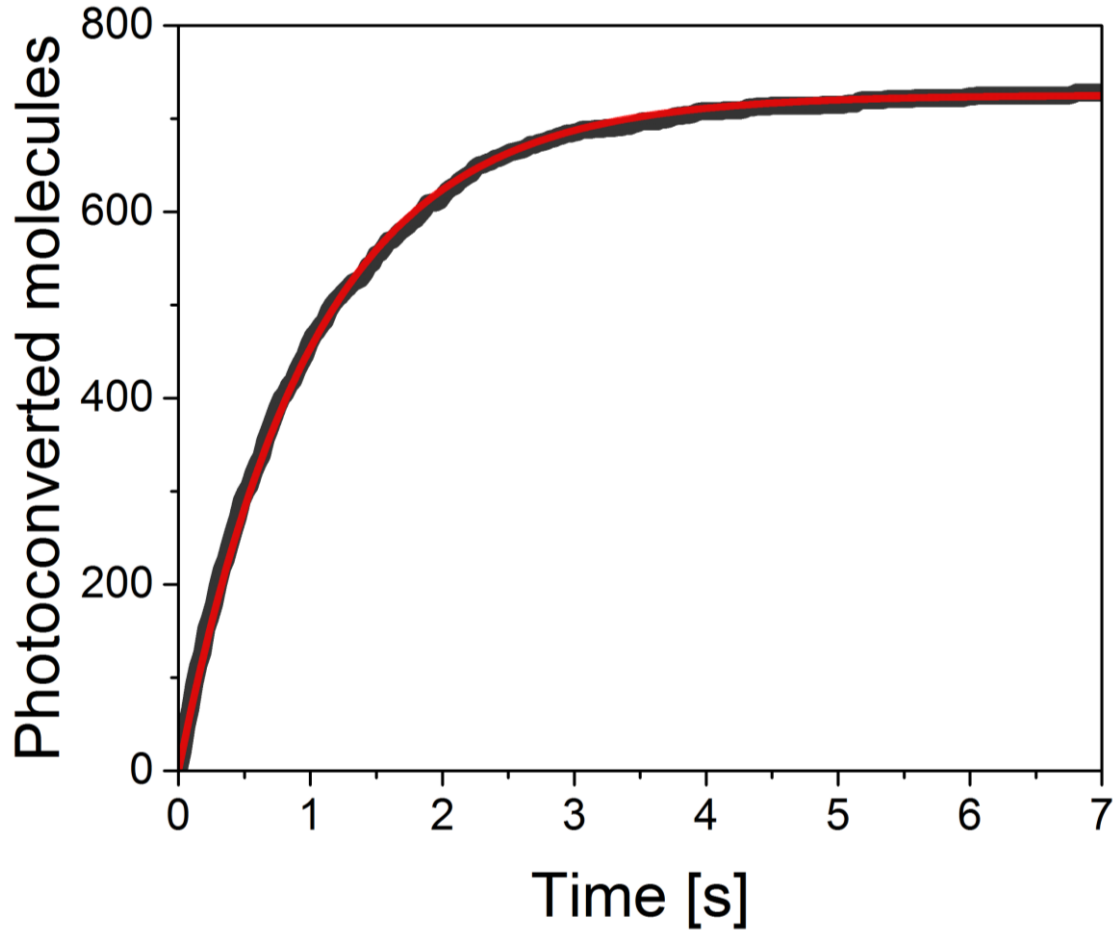

Figure S14. A cumulative photoconversion curve from simulated PALM data without dark state formation in green mEos2 and with high laser heterogeneity can be fitted with a kinetic model that does not incorporate dark-state formation.

A cumulative curve was obtained by processing simulated PALM data (black) in which molecules with a one-to-one green-to-red photoconversion behavior were submitted to activation by a spatially heterogeneous laser. The simulated data were fitted with a kinetic model not accounting for dark-state formation (red). The model accounts well for the simulated experimental data. Hence, averaging the number of photoconverted molecules over regions of different laser densities does not make the cumulative curves significantly biphasic.

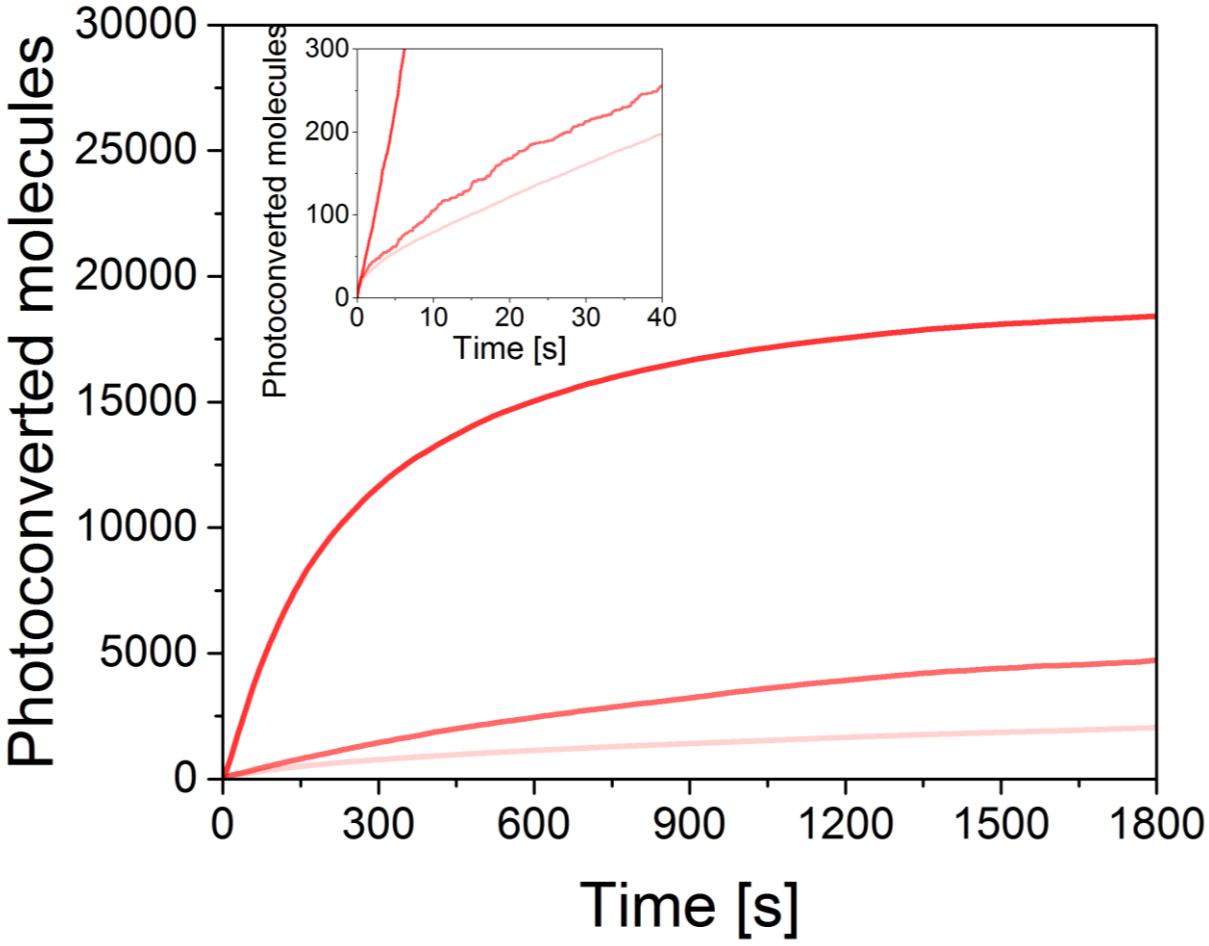

Figure S15. Influence of 405-nm illumination intensity on cumulative photoconversion curves.

Cumulative photoconversion curves of mEos2 embedded in PVA under constant 561-nm readout illumination (2400 W/cm^2) and varying 405-nm illumination (darker shades correspond to higher power densities: 0, 0.03 and 0.8 W/cm^2). Higher power densities of 405-nm light speed up photoconversion, and tend to decrease the biphasic character of the cumulative curves, although a full monophasic shape is never reached. Details of the early progression of the curves are highlighted in the inset.

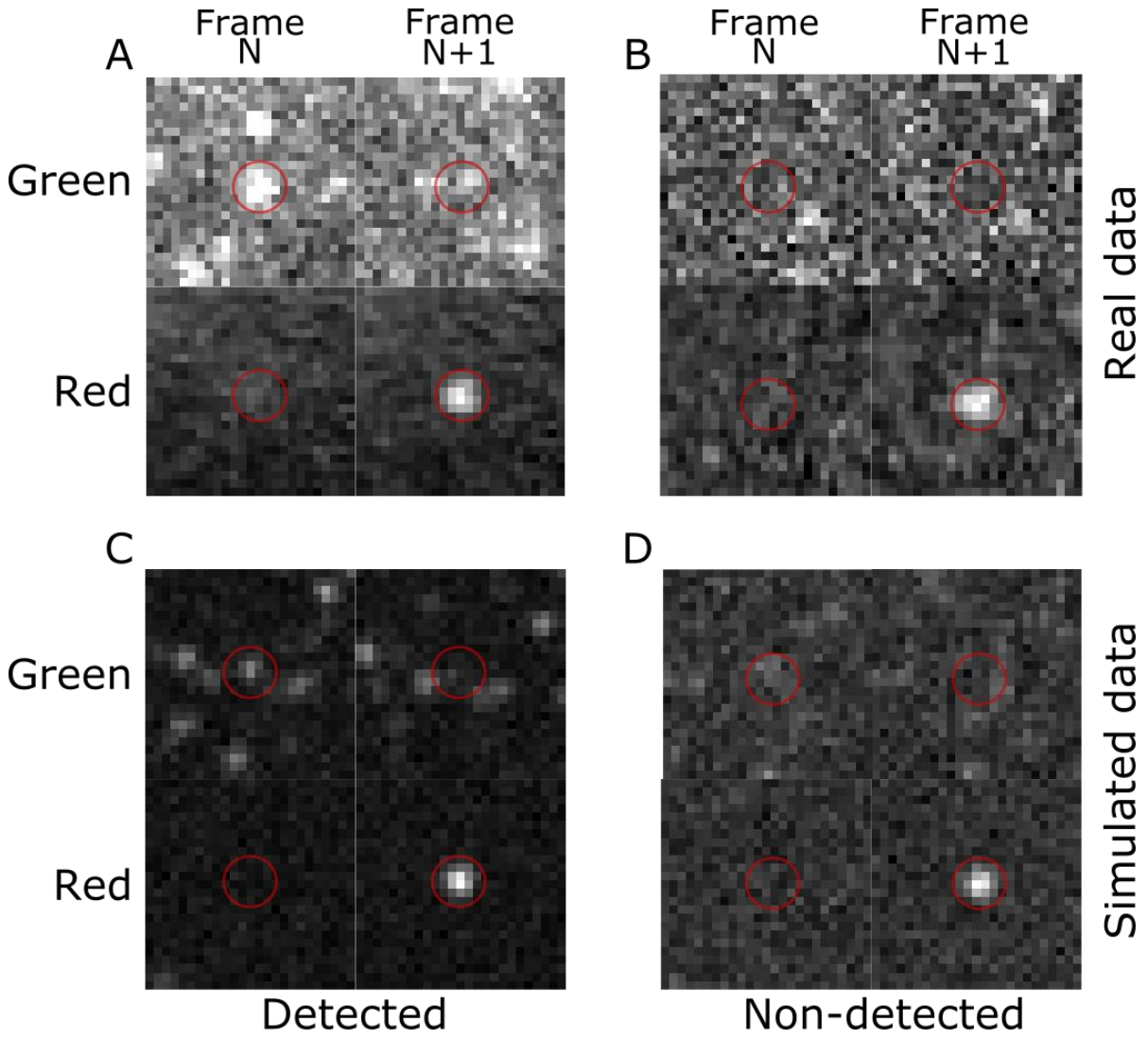

Figure S16. Poor detection of the green ancestors of newly appearing red molecules.

mEos2 embedded in PVA was imaged using a 2-color setup (A,B), under alternating 488- and 561-nm readout light (1200 and 2400 W/cm^2, respectively) and constant 405-nm light (0.8 W/cm^2) or simulated in the same conditions (C, D).

(A, C) Despite a low signal-to-noise ratio, the red molecule appearing at frame N+1 has a green ancestor visible at frame N.

(B, D) No green ancestor can be detected at frame N, because of the poor contrast due to significant back-switching of dark mEos2.

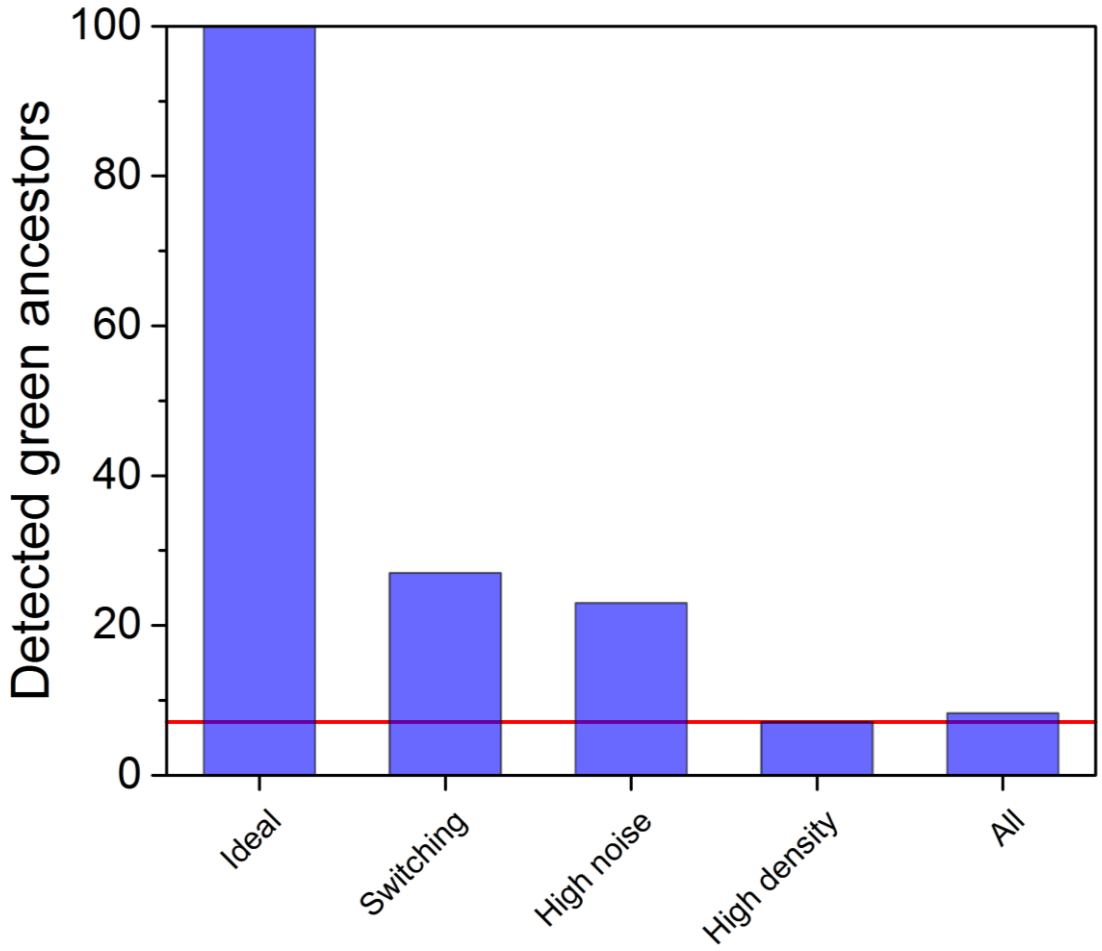

Figure S17. Investigation of causes for poor detection of the green ancestors of newly appearing red molecules.

2-color single-molecule datasets were simulated thanks to an in-house made Matlab-based simulation software. In ideal conditions (no background noise, no fluorophore off-switching in green state, low molecular density), 100% of the green ancestor molecules can be detected. When these factors are individually included in the simulation at levels comparable to experimental conditions, the number of detected ancestors is reduced, with high molecular density having the most drastic effect. If all three parameters are included in the simulation, faithfully reproducing experimental conditions, the level of detection of green ancestors is close to the one observed experimentally (8%, red line).

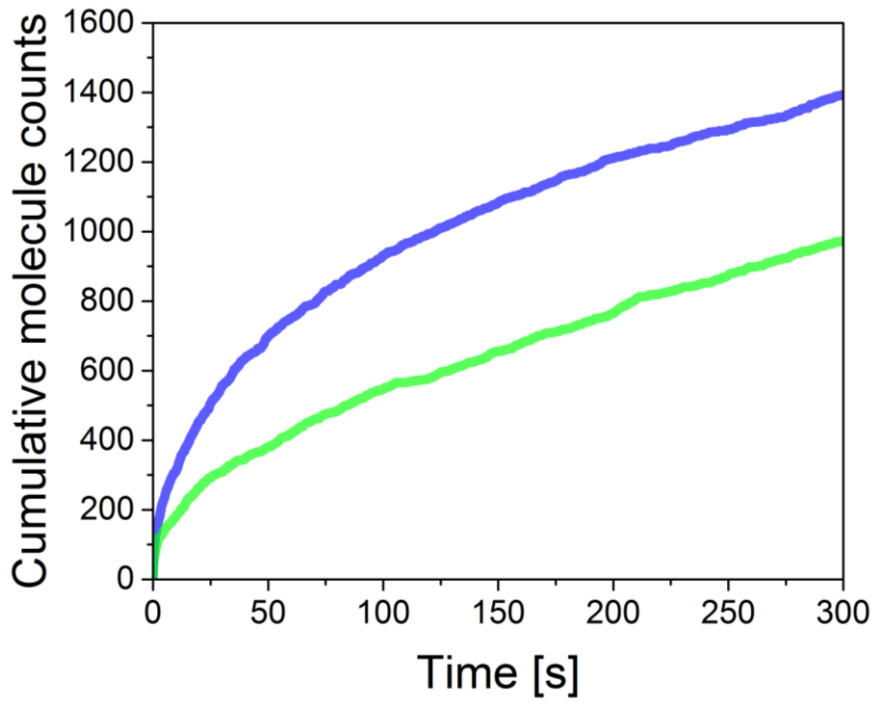

Figure S18. Cumulative curves of red photoconverted molecules under 561-nm illumination only, or alternating 488- and 561-nm illumination.

mEos2 embedded in PVA was imaged under 561-nm readout light, without (green curve) or with (blue curve) alternating 488-nm illumination. Both curves show a clear biphasic behavior, consistent with an important shelving of molecules in D_{long}. However it appears that significantly more molecules get photoconverted in the presence of 488-nm light (despite faster dark-state formation), pointing to substantial light-induced photoconversion at this wavelength.

SUPPLEMENTARY DISCUSSION

Evaluation of spurious effects that could influence the shape of the ensemble switching curves

The shape of the green fluorescence on-off switching curves under illumination at 488 or 561 nm (Figure 1) could be influenced by various causes of heterogeneity in the fluorescent protein population. We have addressed three reasons unrelated to dark state formation that could be at the origin of the observed behavior.

Limited diffusion of the mEos2 molecules in the PVA matrix (Figure S8) was tested by photoconverting a defined region by a short pulse (20 ms) of 405-nm light. The half-width at half maximum of the Gaussian-shaped photoconversion trace was then recorded at regular intervals for 2500 seconds. No significant variation of this value was found over the timespan of the experiment, leading to the conclusion that mEos2 molecules do not diffuse in the PVA matrix over the course of an experiment.

Limited tumbling of the mEos2 fluorophores was addressed by fitting the experimental data with a model taking dipole orientation into account (Figure S9). The obtained fit was however not significantly better, and did not account for the observed decay kinetics.

A possible effect of laser heterogeneity was ruled out, since analyses of the fluorescence levels in ensemble experiments were performed on a small region of the field of view, hence exposed to homogenous laser intensities.

We thus concluded that the shape of the recorded switching curves was to be essentially attributed to the photophysical behavior of mEos2.

Possible artifacts that could lead to deviation of the single-molecule cumulative curves from a monophasic behavior

In order to check if the shape of the single-molecule cumulative curves under illumination at 561 nm (Figure 3A, C) could be affected by spurious effects, possible contamination by impurities was investigated and the effect of laser heterogeneity and fluorophore tumbling were re-examined.

Figure S12 shows a very low level of contamination by impurities in PVA samples, allowing us to attribute the shape of the observed cumulative curves mainly to the contribution of mEos2 molecules. Concerning the laser heterogeneity issue, performing single-molecule analyses on different areas of the field of view corresponding to homogenous laser intensity regions (described in Figure S11) yields local cumulative curves that all exhibit a biphasic behavior. These curves cannot be fitted by a global monophasic model (Figure S13A), but they can be properly fitted with a global biphasic model (Figure S13B). On the other hand, a PALM dataset simulated assuming a highly heterogeneous laser and not incorporating a reversible dark state yields a cumulative curve that can be well fitted with a monoexponential model (Figure S14). Taken together, these results indicate that the biphasic behavior observed experimentally mostly results from genuine green mEos2 photophysics.